JMEPEG (2005) 14:351-355
DOI: 10.1361/10599490523995

1059-9495/$19.00

The Effect of Residual Stresses Induced by Prestraining on Fatigue Life of Notched Specimens

R. Sadeler, A. Ozel, I. Kaymaz, and Y. Totik

(Submitted March 15, 2004; in revised form March 21, 2005)

The effect of tensile prestraining-induced residual stress on the fatigue life of notched steel parts was investigated. The study was performed on AISI 4140 steel. Rotating bending fatigue tests were carried out on semicircular notched specimens with different notch radii in the as-quenched and tempered conditions. Metallography of the specimens was performed by means of light optical microscopy. The finite-element method was used to evaluate the residual stress distribution near the notch region. Fatigue tests revealed fatigue life improvement for notched specimens, which changes depending on the notch radii and applied stress. Scanning electron microscopy was used to examine the fracture surfaces of the specimens.

Keywords finite-element analysis, prestraining, residual stress, rotating bending fatigue

1. Introduction

In most engineering structures, fillets, grooves, notches, and holes are always present, and fatigue cracks will preferentially form at these sites where the local stress is the highest. Designers can never eliminate all stress concentrators in structural components; however, the negative effects of stress concentrators can be reduced by different means, one of which is the compressive residual stresses.

Compressive residual stresses in the surface region of materials with medium and high hardnesses increase the fatigue life and the fatigue limit during cyclic loading compared with materials that are free of residual stresses (Ref 1-10). Residual stresses are introduced in metallic components either intentionally via shot-peening or prestraining, or unintentionally by most metal-forming, metal-cutting, and fabrication processes such as forging, rolling, milling, and welding. These processes introduce residual stresses as a result of inhomogeneous plastic deformation due to mechanically or thermally induced loads (Ref 11).

The importance of residual stresses on the fatigue behavior of metallic components has been demonstrated by a number of authors. Landgraf and Chernenkoff (Ref 12) examined the effects of mechanical and thermal-processing methods, in which large compressive stresses are imparted in the surface layers, on the fatigue behavior of smooth SAE 5160 steel specimens. The results of fatigue tests in notched bending samples of high-strength steel were described with emphasis on the effects of residual stress on fatigue life (Ref 13).

Underwood (Ref 14) described three methods (i.e., press-fitting, tensile prestraining, and shot-peening) of introducing plastic deformation at a notch and in the residual stresses that were produced in A723 steel, and to give the results of notch fatigue tests with the three types of notch treatment. He found that the compressive residual stress increased the fatigue life, and these increases were largest in the prestraining, the residual stress distributions of which were estimated using elastic-plastic stress calculations.

The role of compressive prestresses on notched A542-3 steel specimens subjected to fully compressive cycling was investigated. It was found that the amplitude of the prestress played a decisive role in determining the rate and total distance of crack advance (Ref 15).

Toparli et al. (Ref 16) used finite-element analysis to calculate the residual stresses from prestraining and cold-expansion around notches in low-carbon steel, and attempted to correlate these stresses with measured fatigue lives.

In this study, rotating bending fatigue tests were conducted on both non-prestrained and prestrained cylindrical specimens with different notch radii. Due to the difficulty of experimentally measuring the residual stress at notches with small radii, residual stress distributions around the notch region after prestraining were calculated using finite-element analysis. The increases in the measured fatigue life were correlated with the residual stress results obtained from the finite-element analysis.

2. Experimental Characterization

2.1 Materials and Procedures

AISI 4140 steel (42 CrMo4), which is often used in practical applications in the quenched-and-tempered condition, was used in the current experiments. The nominal chemical composition of the steel is given in Table 1.

The quenched-and-tempered condition was produced by austenitizing for 30 min at 870 °C, oil quenching at 50 °C, and then tempering at 430 °C for 1.5 h. The quenched-and-tempered microstructure is shown in Fig. 1. The mechanical properties of the AISI 4140 steel are listed in Table 2. The work-hardening equation necessary for numerical calculations was selected to be:

$$\sigma = \sigma_o + K\varepsilon^n \quad \text{(Eq 1)}$$

where σ_o is the stress at the beginning of plastic deformation,

R. Sadeler, A. Ozel, I. Kaymaz, and **Y. Totik,** Department of Mechanical Engineering, Faculty of Engineering, Ataturk University, 25240 Erzurum, Turkey. Contact e-mail: recepsadeler@yahoo.com.

K is the stress value when $\varepsilon = 1$, and n is the work-hardening exponent.

The shapes and sizes of the plain and notched specimens with different radii ($2r = 2$, $2r = 3$, and $2r = 4$) are shown in Fig. 2 and Table 3, respectively. The minimum diameter of each specimen was 6.4 mm. Because the fatigue behavior is expected to be influenced by surface roughness in addition to the residual stress, the notch surfaces of all specimens were polished mechanically to reduce the negative effect of surface roughness as much as possible. All specimens were heat treated in a vacuum to eliminate residual stresses induced by the polishing.

In the prestraining process, the loading level for the notched specimens was selected so that the nominal stresses in the test section of the notch reached the yield stress, resulting in significant plastic deformation at the notch root.

Fatigue characterization of both non-prestrained and prestrained notched specimens was performed by means of rotating bending fatigue tests carried out on an R.R. Moore testing machine at a frequency of 50 Hz. The tests were terminated when the complete fracture of the specimen occurred.

Curves of σ_a versus N (Fig. 3) of both the plane and the notched specimens were determined on the basis of 31 tests. In particular, the staircase method (Ref 17) was used to derive the fatigue limit, whereas in the finite life region the 50% survival probability curve was obtained by least-squares fitting method using the following relationship:

$$\sigma_a = CN^{-1/K} \quad \text{(Eq 2)}$$

where σ_a is the fatigue strength, C and K are the fatigue strength coefficient and exponent, respectively, and N is the number of cycles to failure.

By considering the values of the fatigue limit for specimens with different radii, the lower alternating stress level is shown in the σ_a-N curves in Fig. 4 at which fractures were determined. Then, the σ_a-N curves where an improvement in fatigue life due to prestraining occurs can be observed by comparing the fatigue life for the non-prestrained and prestrained specimens. These were determined on the basis of a total of 16 tests, with four tests conducted at each stress level, and by varying the applied alternating stress level (σ_a).

Table 1 Chemical composition of AISI 4140 steel

	Chemical composition, wt.%							
Steel	**C**	**Si**	**Mn**	**P**	**S**	**Cr**	**Mo**	**Ni**
AISI 4140	0.3954	0.225	0.785	0.0187	0.0070	0.847	0.166	0.0795

Table 2 Details of the mechanical properties produced from the heat treatment

Steel	σ_y, **MPa**	σ_{UTS}, **MPa**	ε_f, **%**	K, **MPa**	n	E, **MPa**	σ_o, **MPa**
AISI 4140	1156	1220	16	2319	0.82	210×10^3	1150

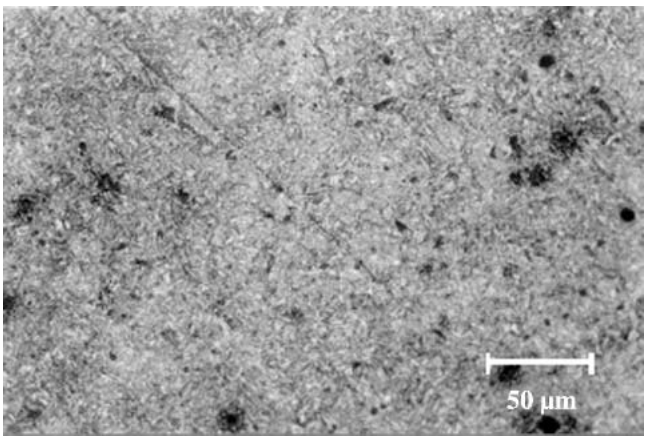

Fig. 1 Microstructure of AISI 4140 steel (etched with 2.5% nital)

3. Fatigue Results

The results of the rotating bending fatigue tests for unnotched and non-prestrained specimens are shown in Fig. 3. The unnotched specimens showed a fatigue limit of 607 MPa. The fatigue limits for the specimens with notch radius of $2r = 2$ mm, $2r = 3$ mm, and $2r = 4$ mm were found to be 356, 389, and 420 MPa, respectively.

Figure 4 shows the σ_a-N curve for non-prestrained and prestrained specimens. The results clearly indicate the beneficial effects of prestraining. At 368 MPa, for instance, the specimens with the notch radius of $2r = 2$ mm showed an improvement of about 36% in fatigue life. The specimens with a notch radius of $2r = 3$ mm showed an improvement of about 20% in fatigue life at the stress level of 405 MPa. Similarly, at 435 MPa, the specimens with a notch radius of $2r = 4$ mm showed only a 13% improvement in fatigue life, which is the lowest. When relatively high alternating stresses (σ_a) were used, the improvement in fatigue life decreased, depending on the increase in the alternating stresses for each specimen with different notch ra-

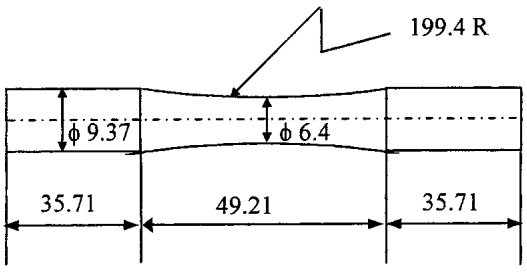

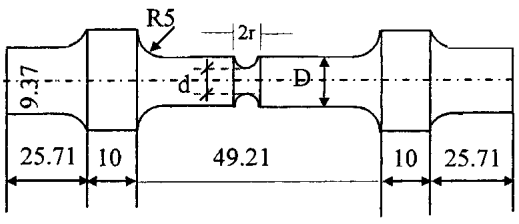

Fig. 2 Shapes of plain and notched specimens (in millimeters)

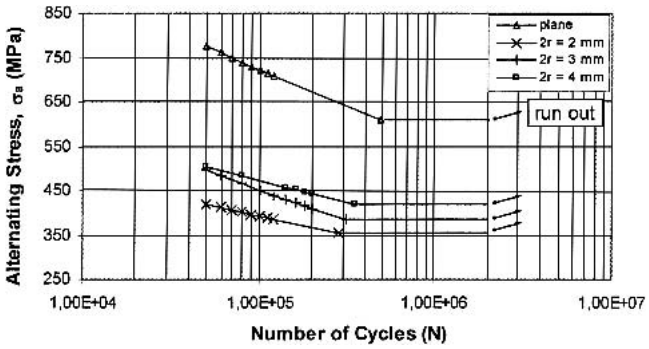

Fig. 3 Rotating bending fatigue curves for plain and nonprestrained notched specimens

Table 3 The sizes of notched specimens

	2r, mm	*d*, mm	*D*, mm
AISI 4140	2	6.4	8.4
AISI 4140	3	6.4	9.4
AISI 4140	4	6.4	10.4

dii. This comparatively modest improvement is attributed to the pattern of residual stresses that tends to fade more rapidly under high alternating stresses (Ref 18).

The fatigue fractures in the notch specimens have previously been observed to originate in the center surface of the notches, which is the critical region due to stress concentration (shown in Fig. 5a). In addition, it was seen from Fig. 5(b) that the compressive residual stresses have affected the critical region, moving it toward the edge of the notch where the magnitude of the compressive residual stresses are lower compared with the center surface of notches.

4. Numerical Calculation

4.1 Calculation of Residual Stresses

Residual stresses occurring after prestraining were calculated by the finite-element method. Because this is an elastic-plastic problem, the initial stress method developed by Zienkiewicz et al. (Ref 19) was chosen.

The fundamental relationships of this method are obtained from the state of uniaxial tension in the elastic-plastic region. Later, these relationships are transferred to the two- and three-dimensional stress cases. For a tensile specimen loaded just past the elastic region ($\varepsilon = \varepsilon_1$), the true stress, σ_{s1}, at ε_1, which is shown in Fig. 6, is given in the following form:

$$\sigma_{f1} = \sigma_1 - \sigma_{s1} \quad \text{(Eq 3)}$$

By using σ_{f1}, the increasing stress value becomes:

$$\sigma_2 = \sigma_1 + \sigma_{f1} \quad \text{(Eq 4)}$$

which corresponds to ε_2. The stress difference between σ_2 and true stress at ε_2 gives σ_{f2}. σ_3 is obtained by replacing σ_{f2} in Eq 3. The following iteration steps lead to the point corresponding to the elastic-plastic strain ε_n and σ_1, where σ_{fi} is the initial stress. Thus, the initial stress cannot be exactly described, as in

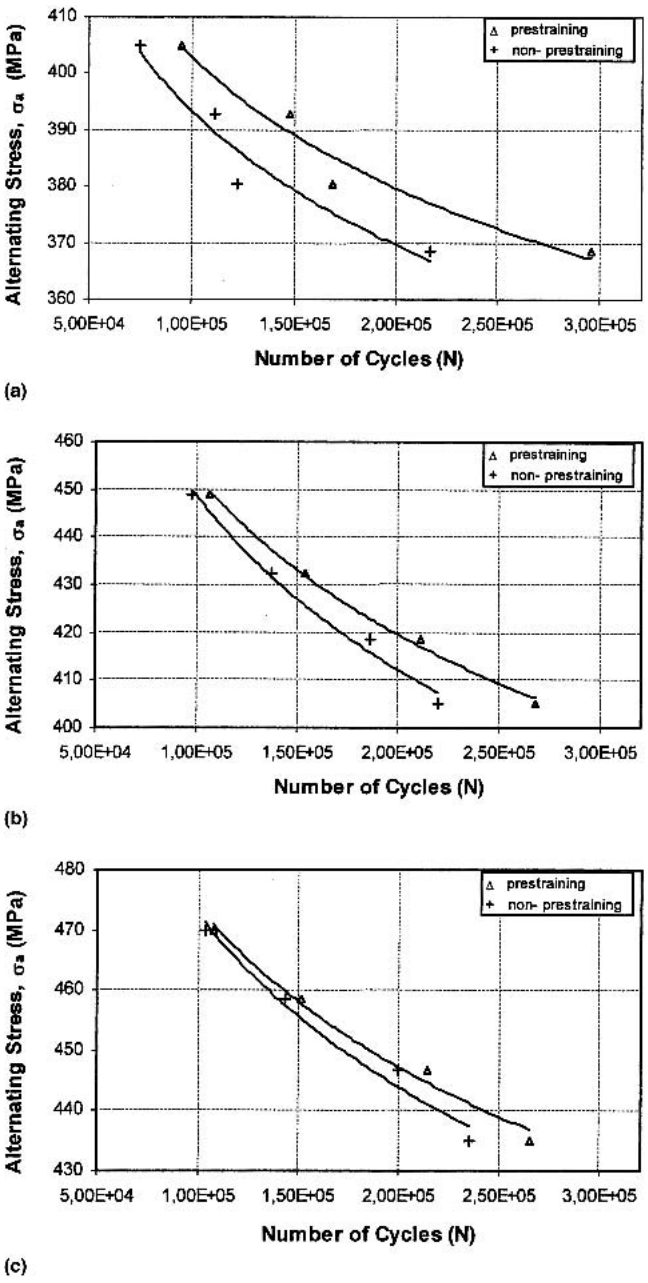

Fig. 4 σ_a-*N* curves for different notch radii: (a) 2r = 2 mm; (b) 2r = 3 mm; and (c) 2r = 4 mm

Fig. 6 in the two-dimensional case. It can be mathematically described, however, as:

$$\{\sigma_f\} = \{\sigma_{fx}, \sigma_{fy}, \sigma_{fxy}, \sigma_{fz}\} \quad \text{(Eq 5)}$$

where σ_{fx}, σ_{fy}, σ_{fxy}, and σ_{fz} are components of the initial stress in the two-dimensional case. The loading stress state that occurs during prestraining can then be written as:

$$\{\sigma\} = \{\sigma_x, \sigma_y, \sigma_{xy}, \sigma_z\} \quad \text{(Eq 6)}$$

By using the following formula, the initial stress components are obtained:

$$\{\sigma\} = \{\sigma\}\frac{\sigma_f}{\sigma} \quad \text{(Eq 7)}$$

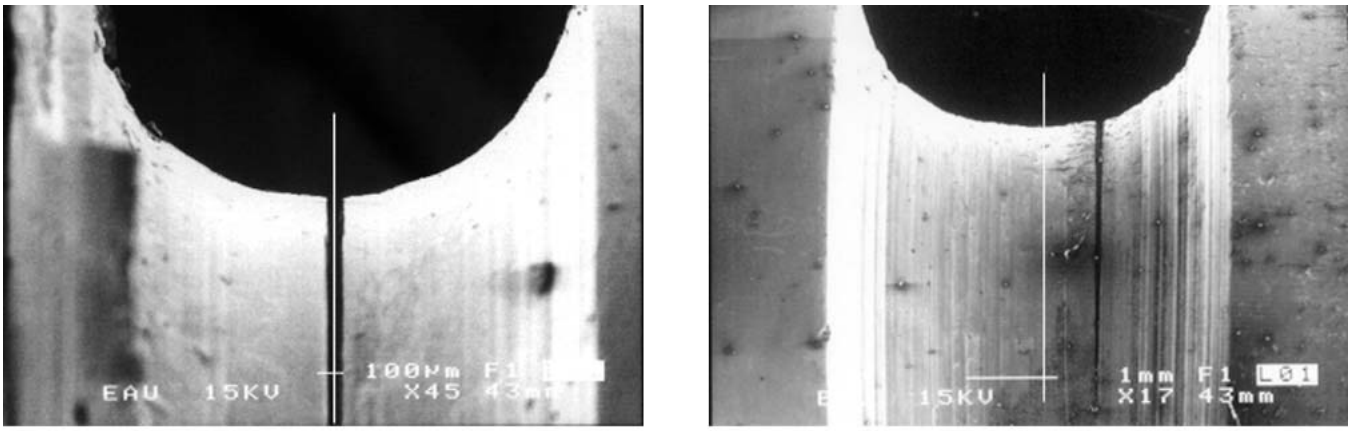

(a) (b)

Fig. 5 Scanning electron micrographs showing the morphology of a crack path initiated from (a) the notched center of non-prestraining treatment and (b) the rim of the prestraining treatment (2r = 2 mm)

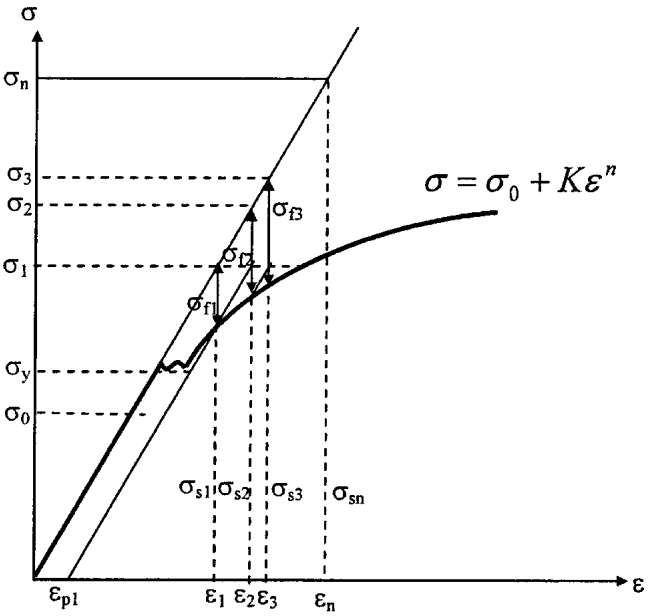

Fig. 6 Initial stress method in the one-dimensional case

where σ_f and σ are the equivalent initial and loading stresses, respectively. In the calculation of the equivalent stresses, the von-Mises yield criterion was used, and, thus, the loading corresponding to the initial stress can be written as:

$$\{P\}_{\sigma_f} = \int [B]^T \cdot \{\sigma_f\} \cdot dV \quad \text{(Eq 8)}$$

where [B] is the strain-displacement matrix and V is the volume. First, the solution displacement vectors $\{\delta_1\}$ are calculated for $\{P\}\sigma_{f1}$, and then the mechanical loading in the first iteration step can be written as:

$$\{\delta_1\} = [K]^{-1}(\{P\}_{\sigma_{f1}} + \{P\}) \quad \text{(Eq 9)}$$

In Eq 9, [K] and {P} are the stiffness matrix and the loading vector, respectively. The iteration steps $\delta_I = 1, 2, \ldots, n$ are then calculated until there is a negligible difference between $\{\delta\}_i$ and $\{\delta\}_{I+1}$. At this point, the displacement vector becomes:

$$\{\delta\}_n = [K]^{-1}(\{P\} + \{P\}_{\sigma_{fn}}) \quad \text{(Eq 10)}$$

And finally, the loading stress $\{\sigma\}_n$, corresponding to $\{\delta\}_n$ in the elastic-plastic region, is calculated as:

$$\{\sigma\}_n = [D] \cdot [B] \cdot \{\delta\}_n - \{\sigma_f\}_n \quad \text{(Eq 11)}$$

In Eq 11, [D] is the elasticity matrix.

For the calculation of the residual stresses, the elastic-plastic loading stress $\{\sigma\}_n$, is calculated first. In the second step, the elastic stress $\{\sigma\}_{el}$ is obtained under the same level of loading to preserve equilibrium. Then, the residual stress is calculated:

$$\{\sigma\}_{res} = \{\sigma\}_n - \{\sigma\}_{el} \quad \text{(Eq 12)}$$

The calculation of the residual stress was performed on a quarter segment of the prestrained specimen due to symmetry, and the finite-element mesh consisted of 600 eight-node isoparametric elements, as shown in Fig. 7. The mesh in the surface region of the notch root was particularly refined with the purpose of better reproducing the residual stresses.

The *y*-components of the residual stress along the *x*-axis, $\sigma(x)_{res,y}$, are plotted in Fig. 8. The residual stresses are believed to give useful information on the effects of residual stress depth and surface magnitude in the notch region during fatigue.

When the largest magnitude of compressive residual stress was considered at the notch surface for each notch radius, it was observed that specimens with a notch radius of 2r = 2 mm exhibited about a 250 MPa larger magnitude in the compressive residual stress than specimens with the notch radius equal to 3, and about a 405 MPa larger magnitude than the specimens with the notch radius equal to 4 mm. The difference between the magnitudes of the compressive residual stresses for the notch radii that are equal to 3 and 4 mm is about 155 MPa. However, the depth of the compressive residual stress for specimens of notch radii equal to 3 and 4 mm are relatively high compared with the specimen with a notch radius equal to

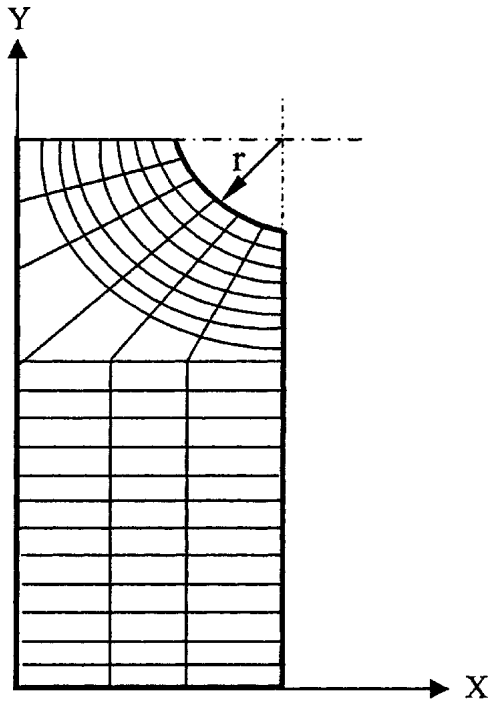

Fig. 7 A quarter of the specimen with the mesh model

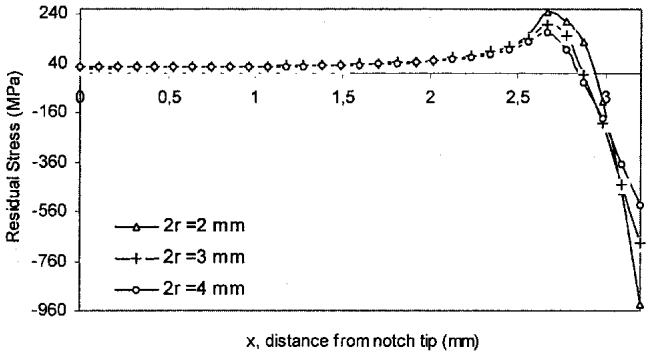

Fig. 8 Residual stress $\sigma(x)_{res,y}$ along the x-axis after the prestraining process

2 mm, but their values are almost the same. For the prestrained notched specimens with a notch radius equal to 2 mm, which had a relatively high surface-level residual stress and a relatively low depth, the fatigue life increment at the lowest alternating stress was among the highest. These results indicate that the surface compressive residual stress is more important than the depth of residual stress for an improvement in the fatigue life. When the results of the all fatigue tests were considered, as well as the distributions mentioned above of the compressive residual stresses, it was found that the sharper the notch, the more effective was the prestraining process and the higher was the fatigue life increment.

5. Conclusions

An experimental and numerical investigation of fatigue behavior of prestrained specimens with different notch radii was presented. From the results, the following conclusions can be drawn:

- A prestraining treatment considerably enhances the fatigue life of the notched specimens. This is due to the presence of the compressive residual stresses in the vicinity of the notch root.
- Prestraining resulted in widely different depths and surface values of the residual stress near the notch root surface, leading to different fatigue lives, depending mainly on the magnitude of the compressive residual stress at the notch root surface.
- The greatest life improvement was obtained for specimens with a notch radius of 2 mm. Thus, the sharper the notch, the more improvement in fatigue life that can be obtained.

References

1. H. Wohlfahrt, Shot Peening and Fatigue of Materials, *Proc. Int. Conf. Shot Peening 1,* A. Niku-Lari, Ed., Pergamon Press Oxford, 1982, p 257-262
2. M. Desvignes, G. Gentil, and K. Habou, Fatigue Behavior of Shot Peened Steel, *Proc. Int. Conf. Shot Peening,* H. Wohlfahrt, R. Kopp, and O. Vöhringer, Ed., Garmisch Partenkirchen, 1987, DGM-Informationsglsellsschoft oberursel, p 369-376
3. Y.H. Yu, The Effect of Shot Peening on Strain Controlled Fatigue Behaviours, *Proc. Int. Conf. Shot Peening 4,* K. Lida, Ed., The Japan Society of Precision Engineering, 1990, p 411-418
4. A. Bigonnet, Fatigue Strength of Shot-Peened Grade 35NCD15 Steel: Variation of Residual Stresses Introduced by Shot-Peening According to Type of Loading, *Proc. Int. Conf. Shot Peening 3,* H. Wohlfahrt, R. Kopp, and O. Vöhringer, Ed., Garmisch-Partenkirchen, 1987, DGM-Informationsglsellsschoft oberursel, p 659-666
5. J.K. Gregory and L. Wagner, Selective Surface Aging to Improve Fatigue Behavior in a High-Strength Beta Titanium Alloy, *Proc. 5th Int. Conf. on Fatigue and Fatigue Threshold,* EMAS Publishing, England, 1993, p 177-182
6. Z. Dingquan, X. Kewei, and H. Jiawen, Aspect of the Residual Stress Field at a Notch and Its Effect on Fatigue, *Mater. Sci. Eng., A,* Vol 136, 1991, p 79-83
7. L. Bertini and V. Fontanari, Fatigue Behavior of Induced Hardened Notched Components, *Int. J. Fatigue,* Vol 21, 1999, p 611-617
8. Z. Xu, H. Jiawen, and H. Zhou, Effect of Residual Stress on Fatigue Behavior of Notches, *Fatigue,* Vol 16, 1993, p 337-344
9. X. Kewei, H. Naisai, and Z. Huijiu, Prediction of Notch Fatigue Limits in a Compressive Residual Stress Field, *Eng. Fract. Mech.,* Vol 25 (No. 2), 1996, p 171-176
10. G.E. Dieter, *Mechanical Metallurgy*, McGraw-Hill, New York, 1986
11. D.W. Hammond and S.A. Meguig, Crack Propagation in the Presence of Shot-peening Residual Stresses, *Eng. Fract. Mech.,* Vol 37, 1990, p 387-390
12. R.W. Landgraf and R.A. Chernenkoff, Residual Stress Effects on Fatigue of Surface Processed Steels, STP 1004, ASTM Intl., R.A. Chernenkoff, Ed., 1996, 571-575
13. J.H. Underwood and J.F. Throop, "Residual Stress Effects on Fatigue Cracking of Pressurized Cylinders and Notched Bending Specimens," Proc. SESA Spring Meeting, 1980
14. J.H. Underwood, Residual-stress Effects at a Notch Root in A723 Steel to Extend Fatigue Life, *Exp. Mech.,* Vol 35, 1995, p 61-65
15. P.B. Aswath, S. Suresh, and D.K. Holm, Load Interaction Effects on Compression Fatigue Crack Growth in Ductile Solids, *J. Eng. Mater. Technol.,* Vol 110, 1988, p 278-285
16. M. Toparli, A. Özel, and T. Aksoy, Effect of the Residual Stresses on the Fatigue Crack Growth Behavior at Fastener Holes, *Mater. Sci. Eng., A,* Vol 225, 1997, p 196-203
17. S.K. Lin, Y. Lee, and M. Lu, Evaluation of the Staircase and the Accelerated Test Methods for Fatigue Limit Distributions, *Int. J. Fatigue,* Vol 23, 2001, p 75-83
18. J.E. Campbell, "Shot Peening for Improved Fatigue Properties and Stress Corrosion Resistance," Report MC1C-71-02, Metals and Ceramics Information Center, Columbus, OH, 1971
19. O.C. Zienkiewicz, S. Valliapand, and I.P. King, "Elasto-plastic Solutions of Engineering Problems 'Initial Stress' Finite Element Approach," *Int. J. Numer. Methods Eng.,* Vol 1, 1969, p 95-100